

Full-scale laboratory testing of a buried pipeline in sand subjected to cyclic axial displacements

B.B. Sheil¹, C.M. Martin¹, B.W. Byrne¹, M. Plant², K. Williams³ & D. Coyne⁴

¹ Department of Engineering Science, University of Oxford, Parks Road, Oxford OX1 3PJ, UK

² Atkins, Woodcote Grove, Ashley Road, Epsom, Surrey KT18 5BW, UK

³ Petrofac, Chester House, 76-86 Chertsey Road, Woking, Surrey GU21 5BJ, UK

⁴ Blackrockpm, Savoy Hill House, 7-10 Savoy Hill, London WC2R 0BU, UK

ABSTRACT

This paper describes a full-scale laboratory study of the axial sliding behaviour of a trenched pipeline surrounded by sand backfill. Cyclic axial displacements are applied to a heavy pipe buried in a narrow trench (less than three pipe diameters wide), using various backfill cover depths and two different soils: dry Hostun sand and a damp silty sand. A novel testing tank is employed, with compressible foam seals to allow the pipe to settle as it moves axially, and a pressure bag system to simulate backfill depths exceeding the height of the tank. The test pipe is instrumented to measure (a) the axial soil resistance developed on an isolated central section of pipe (thus avoiding tank boundary effects), and (b) the normal and shear contact stresses at a number of points around the pipe circumference. The results indicate that both the axial resistance and the normal stress distribution around the pipe can undergo considerable changes when a pipeline experiences cyclic axial displacements. An extreme case identified here is the potential for a compacted damp sand backfill to ‘arch’ completely over the pipe as a result of differential settlement, leading to unexpectedly low axial resistance. To address some limitations of the design method currently used in industry, a new approach for estimating axial resistance is suggested and applied to the present test data.

1 INTRODUCTION

2 Pipelines are frequently buried to protect them from frost and above-ground activities. The
3 backfill soil surrounding the pipe is a source not only of transverse restraint (in the downward,
4 upward and lateral directions) but also of axial restraint. Buried pipelines that carry hot fluids
5 experience thermally-induced axial expansion, and in such cases the magnitude of the axial
6 soil resistance is critical:

- 7 (a) too little and the pipeline can experience large end expansions, in turn disturbing the
8 surrounding soil and complicating the design of expansion control devices;

(b) too much and the pipeline can experience failure through excessive axial stress in the pipe wall, or by global buckling failure (e.g. upheaval buckling).

Pipelines carrying hot fluids are typically subject to periodic start-ups and shut-downs, as well as operating and diurnal temperature fluctuations, resulting in cyclic axial displacements and axial stress variations (Bilgin & Stewart, 2012). The cyclic nature of the axial loading affects the soil response and can result in fatigue damage to the pipeline (Cullin et al., 2015). Quantifying the likely range of axial soil resistance over the life of the pipeline, accounting for the influence of the cyclic loading history, is essential when designing a buried pipeline for various limit states (serviceability, ultimate, fatigue) as well as for buckling prevention and economy.

The widely used design guideline for onshore buried steel pipelines, ALA-ASCE (2001), provides the following expression for calculating drained axial resistance:

$$R_a = \gamma' H \cdot \frac{1 + K_0}{2} \cdot \tan \delta \cdot \pi D \quad (1)$$

where R_a is the axial resistance per unit length, γ' is the effective unit weight of the backfill soil, H is the depth of soil cover measured from the pipe springline, K_0 is the coefficient of lateral earth pressure at rest for the soil, δ is the pipe–soil interface friction angle, and D is the external pipe diameter. Equation (1) is effectively a simple Coulomb friction model based on the assumption that the upper and lower quadrants of the pipe are subject to the *in situ* vertical effective stress, with the left and right quadrants experiencing K_0 conditions. The basis for this modelling assumption is not discussed in ALA-ASCE (2001), and numerous studies have identified more complex initial distributions of normal stress around the circumference of a buried pipe (e.g. Brachman et al., 2000; Weidlich & Achmus, 2006; Talesnick et al., 2011; Ahmed et al., 2015).

The ALA approach in equation (1) does not consider several potentially important effects on the axial resistance, such as pipe self-weight, trench boundary effects, the relative density of the backfill soil, and the influence of previous axial displacement cycles. While the model has been shown to be adequate for lightweight pipes buried in loose sand, significant under-predictions have been noted for pipes buried in dense sand (Scarpelli et al., 2003; Anderson et al., 2004; Karimian, 2006). This has been attributed to increases in the initial normal stresses as a result of shear-induced dilation in the interface soil layer surrounding the pipe (Wijewickreme & Weerasekara, 2015). Weidlich & Achmus (2006) noted that for buried pipes in sand, the influence of axial displacement cycles was dependent on the relative density of the backfill. Loose samples showed an increase in axial resistance, while dense samples gave a reduction (with the maximum resistance occurring during the first displacement cycle). These findings were supported by Bilgin & Stewart (2009) in research on the axial response of flexible pipes in dense sand. Huber & Wijewickreme (2014) investigated the influence of a prescribed heating and cooling history on the ultimate axial capacity of a full-scale test pipe buried in moist sand. ‘Arching’ of the soil over the pipe was identified following a sufficient number of heating cycles prior to pullout testing.

This paper describes the development of a laboratory testing apparatus for investigating the axial resistance of a full-scale pipe section buried in sand. Selected results from a test programme carried out to support the design of a commercial onshore gas pipeline are also presented. Important features of the field project are the heaviness of the pipe (of order 400 kg/m due to a thick wall requirement for corrosion resistance), and the need to accommodate large-amplitude axial displacement cycles arising from thermal expansion and contraction. Predictions using the ALA approach for this type of design scenario are unverified. The main objectives of the test programme were to measure the initial normal stresses around the circumference of a heavy steel pipe buried in a narrow trench backfilled with sand, and to

investigate the influence of cyclic axial pipe displacements on (a) the overall axial soil resistance, and (b) the redistribution of contact stresses around the pipe. Predictions determined using the ALA approach are compared with the measured data, and an alternative design methodology is developed based on the results.

TESTING RIG

A new testing rig was designed and built at the University of Oxford specifically for measuring, at full scale, the axial soil resistance developed on a length of buried pipe subjected to cyclic axial displacements. Illustrations of the apparatus are provided in Figs 1 and 2, and the main features are described in the following paragraphs. The instrumented test pipe, which allows accurate measurement of the axial soil resistance as well as the local normal and shear contact stresses at a number of points around the circumference, is described in a separate section below.

Testing tank

The tank frame was constructed using standard structural steel channels and I-beams (see Fig. 1(a)). Because of headroom restrictions in the laboratory, the depth of soil cover in the set-up was limited to a maximum of ~ 1.2 m ($\sim 3.4D$) above the crown of the pipe. The width of the tank was chosen to match the intended trench width of 0.95 m in the field project. The as-built internal dimensions of the tank are given in Fig. 2. The tank was raised onto six 0.5 m high columns to allow soil to flow through a trapdoor in the base of the tank, and onto a conveyor belt to facilitate emptying of the tank. The tank side walls comprised 25 mm thick marine plywood panels that were bolted to the steel frame to minimise lateral deflections during testing. The tank side walls were left rough to mimic trench roughness in the field.

A bespoke pressure bag system was employed to simulate backfill cover depths greater than those achievable using soil within the height of the tank. In these tests the bag reacted against a steel top plate without touching the tank side walls. The top plate was 10 mm thick, with additional web stiffeners to minimise bending during inflation of the pressure bag. The pressure bag was connected to the laboratory compressed air supply, via a regulator. During each test the bag pressure was monitored using an electronic air pressure transducer, and the regulator was manually adjusted to maintain the target pressure (typically to within 1%) throughout the test.

Pipe–tank interface

The heavy pipe was expected to undergo significant settlement into the underlying bed layer of backfill soil during the cyclic axial testing. Therefore a system involving two stiffened steel face plates, each with a compressible foam seal around the pipe, was employed to allow unrestrained settlement of the pipe whilst preventing soil egress (see Fig. 3). Fireseal class 0 open cell polyurethane foam (40 mm thick) was selected for its high compressibility and its ability to rebound rapidly after compression. The amount of settlement available from foam compression was ~30 mm (corresponding to an applied stress of < 10 kPa on the foam). An additional 30 mm was available using slotted holes in the sliding face plates if the pipe settlement approached the maximum foam compression during a test, but this did not occur in any of the tests reported here.

The position of the pipe relative to the tank was monitored by three linear variable differential transformers (LVDTs) with a linear range of 50 mm. Two of these LVDTs were fixed to the tank frame and aligned vertically to measure the vertical displacement at each protruding end of the pipe (allowing calculation of pipe settlement and rotation). The third LVDT was fixed

to the pipe and aligned horizontally to measure the axial displacement of the pipe relative to the tank. Figure 3 shows this arrangement at one end of the tank.

Actuation system

The pipe was pushed and pulled axially through the tank using a 200 kN translating mechanical screw jack, driven by a high torque two-phase stepper motor and gearbox. The jack was connected to the end flange of the pipe spindle through a 200 kN S-beam tension/compression load cell fitted with knuckle joints (see Fig. 1(b)). This load cell is referred to as the external axial load cell, and served as a useful check on the axial resistance measurements obtained from the instrumented central pipe section inside the tank. The elevation of the plate supporting the jack was adjustable relative to the tank through the use of slotted bolted connections in the upright channels (see Fig. 2). These uprights were connected to the testing tank through four horizontal reaction beams, which were dowelled into the tank frame to minimise relative movement under the high axial forces developed during the cyclic testing.

INSTRUMENTED TEST PIPE

Pipe structure

To minimise tank boundary effects on the measurement of axial soil resistance, the pipe was split into three sections, with a shorter central section (500 mm long) connected to two longer end sections. The central section was isolated from the end sections by incorporating two sets of axial load cells into the ‘spindle’ support structure running along the inside of the pipe (see Fig. 4). Four 50 kN S-beam tension/compression load cells were used, two located at either end of the central pipe section, attached to the top and bottom of flanges in the spindle. These are referred to as the internal axial load cells, and they allowed the net axial force due to soil

friction on the central pipe section to be determined from the difference between the axial force readings at each end.

The three pipe sections were machined to an outside diameter of 350 mm and a wall thickness of 6 mm, and were separated by small gaps (3 mm wide) filled with a flexible silicone sealant. For this study the central section was coated with Nap Gard 7-2610, a common epoxy coating used for steel oil and gas pipelines to provide improved corrosion resistance and mechanical durability. The average of three profilometer measurements for this coating gave a maximum roughness $R_{\max} = 39.2 \mu\text{m}$, using the relative height between the highest peak and the lowest trough along a surface profile 15 mm in length.

The two end sections were left uncoated. Each pipe section was supported by a series of welded spokes connected to the internal spindle, which was a steel square hollow section ($120 \times 120 \times 10$ SHS). A view of the test pipe during assembly is shown in Fig. 5.

A hanger-and-weights system was developed to allow different pipe weights to be simulated (see Fig. 4). The results presented in this paper focus on an effective pipe weight of 4 kN/m, reflecting the anticipated self-weight of the pipe in the field project. The very high flexural rigidity of the spindle section ensured that minimal bending deflections were induced by hanging weights at the ends of the pipe. This overall beam bending effect should be distinguished from a separate bending effect, namely ovalising of the pipe cross section under large overburden pressures. Such distortion is also expected to be minimal as a result of the robust internal spoke design visible in Fig. 5.

Stroud load cells

Six ‘Stroud’ type contact stress transducers (Bransby 1973; Stroud 1971) were fitted into the central section of the test pipe, as shown in Figs 6 and 7. Each Stroud cell measured the normal force, shear force and moment applied by the soil to a small area of the pipe surface ($40 \text{ mm} \times$

40 mm). The slender strain-gauged webs inside the cells were sized to allow measurement of up to 150 kPa normal stress acting concurrently with 100 kPa shear stress. The Stroud cells were fitted into the face of the central pipe section using individual steel housings that were mounted on the inside of the pipe wall (see Fig. 7). Each cell was equipped with a curved lid machined to a radius of 175 mm, to ensure a flush finish with the outer surface of the pipe (see Fig. 6). The lids were coated with the same Nap Gard epoxy as the central pipe section, and each lid was isolated from the main body of the pipe wall by a 1 mm gap filled with soft silicone rubber. The Stroud cells were aligned to measure shear stresses acting parallel to the axis of the pipe; no attempt was made to measure circumferential shear stresses.

Calibration of each Stroud cell was achieved by keeping two of the three loads N , S and M (normal, shear and moment) constant, whilst varying the third. The procedure followed was similar to that used by Martin (1994). As each of the three loads is varied, the (linear) relationship between the output voltage from each strain gauge circuit and the applied load can be deduced. This provides a 3×3 matrix that can be inverted to allow the loads to be determined from the circuit voltages. In this paper the normal stresses measured by the Stroud cells are denoted σ'_x , where X denotes the location of the Stroud cell according to the key in Fig. 7(a).

EXPERIMENTAL METHOD

Dry sand material and preparation

The dry sand used in the testing was Hostun HN31, the properties of which are well-documented (e.g. Colliat et al., 1986; Flavigny et al., 1990) and are listed in Table 1. The measurements of the peak and critical state friction angles were obtained from triaxial tests on samples with a relative density of 51%, at a confining pressure of 80 kPa. A portable conveyor belt was used to transfer sand from a storage tank to the testing tank. A large weighing scale,

located beneath the storage tank, was used to measure how much soil was added to the testing tank during sample preparation, thus allowing the overall unit weight to be calculated for each sample. The final depth of backfill was determined using a laser distance meter, averaging at least eight readings across the plan area of the sample.

A sand raining box was used to ensure a repeatable sample density for each of the dry sand tests. The rainer was 150 mm deep, with the same internal plan dimensions as the testing tank, and was bolted to the top of the tank during the raining process. Holes were uniformly distributed over the base of the box in a grid layout, and a sliding aluminium sheet drilled with the same pattern was used to open and close the holes, as required. A hole diameter of 10 mm was used to target a loose to medium dense test bed. *In situ* density pots were used to verify the repeatability of the sample preparation, yielding an average relative density of $35\% \pm 2\%$ at the level of the pipe springline (sample size of 12). The raining procedure involved initial placement of a 300 mm deep bed layer, followed by a pause while the pipe was inserted into the tank and laid down on the bed layer, after which raining was resumed until the target cover depth was achieved. The bed layer and the overburden soil were not subjected to any mechanical compaction in the dry sand tests.

Damp sand material and preparation

A number of tests were conducted using a candidate backfill material from the field project site. This material was a damp silty sand and is referred to as “Sand K” henceforth. Properties of the sand are listed in Table 1, with the particle size distribution presented in Fig. 8. Since the damp sand would not flow through the rainer, it was dumped directly into the testing tank from the conveyor to prepare a ‘loose’ sample, while additional vibratory compaction was carried out at intervals to prepare a ‘dense’ sample. These processes reflect extremes of practice that may occur on site.

In all of the Sand K tests discussed, a 300 mm deep bed layer beneath the pipe was prepared with compaction, even if the soil above that level was to be placed in a loose condition. Vibratory compaction was carried out by applying a 400 mm × 320 mm commercial plate compactor to sand placed in layers 100 mm thick, for 15 minutes per layer. However, once the pipe had been laid down on the bed layer and sand placement from the conveyor was resumed, no compaction was permitted until the soil level was 100 mm above the pipe crown. This was to reduce the possibility of vibration-induced damage to the Stroud load cells.

Pipe installation and test set-up

Before the pipe was inserted into the testing tank, a curved profile was scraped into the 300 mm deep bed layer to allow the pipe to sit evenly on the underlying sand. A temporary steel bridge was placed into the tank to support the pipe and prevent disturbance of the bed layer while the pipe was threaded through the holes in the face plates (see Fig. 2). Once the pipe had been inserted, the temporary bridge was removed and the pipe was then lowered using chain blocks at both ends to ensure a horizontal touchdown. When the pipe was resting on the sand, the compressible foam seals were attached and the sliding steel face plates were fixed in position (see Fig. 3).

During the course of the testing, three different configurations were adopted to model various trench conditions and degrees of confinement, as shown in Fig. 9:

- (i) overburden fully replicated with soil cover (limited to cover depths ≤ 1.18 m above the top of the pipe);
- (ii) overburden replicated with 1.1 m of soil cover in conjunction with the pressure bag above an 18 mm thick plywood platen;

(iii) overburden replicated with 0.35 m of soil cover in conjunction with the pressure bag above a 0.7 m thick rigid timber spacing box.

Set-up (i) simulates a narrow trench where there may be some loss of overburden pressure through friction along the walls of the trench, thereby providing a lower-bound measurement of the axial resistance derived from a given depth of soil cover. Set-up (iii) is more representative of a wider trench with sloping sides, where the pipe is likely to experience the full overburden pressure of the overlying soil. This, together with the use of a rigid surcharge boundary condition, provides an upper-bound measurement of the axial resistance. Set-up (ii) is an intermediate condition.

The nominal overburden pressure, σ'_v , acting at the level of the pipe crown was calculated as

$$\sigma'_v = \gamma' h + p_{\text{bag}} A_r \quad (2)$$

where h is the depth of soil cover measured from the pipe crown, p_{bag} is the bag pressure (if applicable) and A_r is the pressure bag area ratio (bag plan area divided by tank plan area). For the pressure bag used in these tests, the area ratio was $A_r = 0.64$, and this was used in equation (2) for test set-ups (ii) and (iii).

An illustration of various boundary and pipe–backfill interaction effects likely to be encountered during the testing programme is provided in Fig. 10. The ‘trench’ effect depicted in Fig. 10(a) refers to a loss of vertical overburden pressure to the tank walls through interface friction. The ‘rigid inclusion’ effect in Fig. 10(b) occurs because the pipe behaves as an effectively rigid body within the compressible soil backfill, and therefore attracts a greater proportion of the overburden pressure. Figure 10(c) shows an accentuated version of the rigid inclusion effect, referred to here as the ‘pinching’ effect, where surcharge pressure is applied through a rigid platen boundary condition close to the pipe crown, as is the case in test set-up (iii). This type of boundary condition would also be expected to accentuate any increase in the

normal stresses on the pipe arising from confined dilatancy during axial movement of the pipe. Finally, Fig. 10(d) depicts a possible scenario where the backfill soil arches over the crown of the pipe.

Testing programme

Table 2 summarises the sample properties and configurations of the tests reported in this paper. These are a subset of a larger programme of tests performed for the industry-funded research project. The tests denoted H1-H4 used dry Hostun sand, whilst K1-K4 used damp Sand K. Each test involved the application of displacement-controlled axial pipe movements, with alternating sets of large-amplitude (20 mm) and small-amplitude (2 mm) cycles, as detailed in Table 3. In preliminary tests to commission the new apparatus (not reported in this paper) the change in the peak axial resistance after five cycles was observed to be minimal. Therefore, the number of cycles selected for the main testing programme was a compromise between (i) mobilising the maximum likely peak resistance in any one cycle set, and (ii) the time taken to perform a test. The large-amplitude cycles represent the main thermally-induced axial displacements during pipeline start-up and shut-down, whereas the small-amplitude cycles correspond to diurnal temperature fluctuations. Following Tests H1 and H2, the test procedure was revised slightly to provide a more expedient examination of the influence of large-amplitude axial displacement cycles (see the final column of Table 3). A different procedure was adopted for Test K4 in order to examine the influence of progressively increasing overburden pressure on the pipe response in the absence of small-amplitude cycles. The sequence for this test is shown in Table 4. In all tests displacement rates of 14 mm/min and 4 mm/min were adopted for the large- and small-amplitude cycle sets, however, rate effects in dry or damp sand are not expected to be significant.

EXPERIMENTAL RESULTS

Typical test results

Representative test results for the initial packet of cyclic axial displacements (cycle set A) are presented in Figs 11 and 12 for Hostun sand (Test H2) and Sand K (Test K2) respectively. Shown in these plots are (a) the load–displacement response for the whole pipe assembly (comprising coated and uncoated steel sections) deduced from the external axial load cell measurements, (b) the load–displacement response for the central (coated) pipe section deduced from the internal axial load cell measurements, and (c) the vertical pipe settlement deduced from the LVDT measurements at either end of the pipe. The pipe rotation deduced from the LVDT measurements is not plotted, but was negligible (less than 0.1°) in both tests.

Figures 11(a) and 11(b) show that for Test H2 the cyclic load–displacement responses are highly symmetrical, and furthermore that the axial resistance measurements for the whole pipe agree very well with those for the isolated central section only. This indicates that the foam seals at the pipe–tank interface induced negligible friction on the pipe. It can also be seen from Fig. 11(c) that the foam allowed unrestrained settlement of the pipe during the axial displacement cycles. Interestingly, the majority of settlement for a given cycle occurs in the first 2–3 mm following a reversal of loading direction. The settlement accumulated in each cycle reduces as the test progresses.

By contrast, for Test K2 there is a notable difference between the axial resistances measured for the first cycle in Figs 12(a) and 12(b). The likely reason for this is rusting (and hence roughening) of the uncoated steel end sections, leading to adhesion of the damp sand to the pipe during backfill placement and compaction. After the first cycle, the adhesion is broken and the axial resistance drops off significantly, approaching the resistance corresponding to frictional sliding of the pipe under its self-weight only (see the dash-dot lines in Fig. 12, which

are plotted for a pipe weight of 4 kN/m and an assumed friction coefficient of $\mu = 0.6$, giving 2.4 kN/m). This suggests that the backfill is arching over the crown of the pipe (Fig. 10(d)), and also that there are negligible normal stresses acting on the sides of the pipe. The arching hypothesis is supported by the observation that the first few reversals of loading direction, where the pipe experiences the greatest settlement, coincide with reductions in the measured axial resistance. By comparison with the data presented in Fig. 11(c) for Hostun sand, the settlements in Fig. 12(c) are notably lower after the first cycle because of (a) the loss of overburden pressure acting on the pipe crown forcing the pipe downwards, and (b) the denser condition of the Sand K bed layer.

Virgin load–displacement response

Figure 13 compares the axial load–displacement curves observed in the first cycle of each test. In this and all subsequent figures the axial load is that measured over the isolated central section of pipe. In the tests with Hostun sand, the nominal σ'_v values at the pipe crown were 6.9, 13.7, 50 and 50 kPa for Tests H1-H4 (see equation (2) and Table 2). Figure 13(a) shows that, as expected, an increase in nominal overburden pressure corresponds to an increase in axial resistance. These results are re-plotted in Fig. 13(b) except that the axial resistance and displacement, R_a and Δ , have now been normalised by $\sigma'_v \pi D$ and D respectively. It is clear that this approach to normalising the resistance, which is similar to that adopted in the ALA approach in equation (1), does not produce satisfactory agreement between tests. For example, the influence of the soil cover height may be examined by comparing Tests H1 (0.5 m cover) and H2 (1.0 m cover). Test H1 gives a higher normalised resistance, the most likely cause being that the normalisation does not account for the ~2.4 kN/m of axial resistance derived from the pipe weight, which is a significant part of the total resistance in Test H1 but less so in Test H2. Between Tests H2 ($\sigma'_v = 13.7$ kPa) and H3 ($\sigma'_v = 50$ kPa) there is an increase in overburden

pressure, applied using pressure bag system, but a reduction in the normalised resistance, indicating that not all of the additional pressure is being transmitted to the pipe (possibly indicating a significant trench effect, Fig. 10(a)). Tests H3 and H4, which involve the same nominal overburden pressure but use set-ups (ii) and (iii) respectively (see Fig. 9), demonstrate the influence of the surcharge boundary condition. The higher absolute and normalised resistances in Test H4 can be attributed to a smaller trench effect (less depth of actual soil cover and hence less loss of surcharge pressure to the trench walls, Fig. 10(a)) as well as the pinching effect of the rigid platen on the pipe (Fig. 10(c)). In general, these results indicate potentially significant influences of pipe weight and trench wall friction on the axial resistance, which may need to be accounted for in design.

Corresponding results for the tests with Sand K are shown in Figs 13(c) and 13(d). The tests where the backfill was compacted (i.e. Tests K2-K4) show a brittle response, with the peak resistance occurring at $\Delta/D < 0.2\%$. This is followed by a significant drop in resistance upon reversal of direction, which as discussed above is due to the initiation of soil arching. By contrast, no distinct peak or drop in resistance is evident for the test with loose backfill (Test K1) because arching did not occur. It is worth remarking that on the return leg, the normalised resistance in the loose test (K1) is more than twice that in the comparable dense tests (K2 and K3). This indicates that backfill compaction may have the opposite effect to that intended, and further experimental research (also considering a range of trench configurations) would be interesting.

Influence of displacement cycles

The influence of axial displacement cycles on peak axial resistance is shown in Fig. 14. Within each cycle, differences between the forward and return resistances were minimal, with the exception of the initiation cycle for arching (see Figs 11 and 12). The average of the peak

resistances from the forward and return legs has therefore been plotted in Fig. 14 against the number of large cycles. The packets of small displacement cycles detailed in Table 3 are indicated with dotted vertical lines.

For the tests with Hostun sand backfill, Fig. 14(a) shows that the axial displacement cycles in Tests H1 and H2 induce a gradual increase in the axial resistance. In particular, a distinct increment in resistance is evident after each set of small cycles, which can be attributed to cyclic densification of the soil immediately surrounding the pipe. Figure 14(b) shows that the same temporary effect of small cycles occurs in Tests H3 and H4, where the pressure bag system was used, but compared with Fig. 14(a) the long-term increase in resistance over the course of the test is less pronounced. The highest resistance for Test H4 occurs in the very first cycle, which may be attributed to the pinching effect of the rigid platen in test set-up (iii) (see Figs 9(c) and 10(c)).

Figure 14(c) shows that for the Sand K loose test (K1) there is a gradual increase in axial resistance with the number of cycles. By contrast, for the Sand K dense tests (K2 and K3), there is a large drop in resistance after the first cycle. Additional axial displacement cycles induce further reductions to the point where the resistance approaches a residual value just above that for frictional sliding under pipe self-weight only. Again, this indicates that the compacted damp backfill is arching over the pipe, with the arch being maintained during several sets of large- and small-amplitude cyclic axial displacements.

Figure 15 shows the influence of the step changes in overburden pressure during Test K4 (through inflation of the pressure bag) on the peak axial resistance, averaged from the forward and return legs of each cycle as before. For the initial set of cycles the resistance again drops to a value close to self-weight frictional sliding of the pipe, indicating the occurrence of arching. However, both of the subsequent bag inflations induce increases in the normalised axial resistance, so the formation and maintenance of an arch therefore appears to be dependent

on the level of overburden pressure. This suggests the possibility of a limiting overburden pressure for the occurrence of arching. It should be noted, however, that the other general trend observed in this figure is for the resistance to decrease with the number of large cycles applied at a given overburden pressure; therefore a continued application of cyclic axial displacements may eventually induce arching.

Contact stresses

Initial normal stress readings from selected Stroud cells are shown in Fig. 16. For each test, measured values of σ'_N at the pipe crown (Fig. 16(a)) and the average of σ'_E and σ'_W at the pipe sides (Fig. 16(b)), immediately prior to axial loading, are plotted against the nominal overburden pressure, σ'_v , at the relevant depth (this is calculated using equation (2) with the appropriate cover depth, h). Measured data from Wijewickreme et al. (2009), for a 457 mm diameter steel pipe buried in dry sand, are also plotted.

In Fig. 16(a), the fact that all of the data points from the present study lie above the 1:1 line confirms the existence of a measurable rigid inclusion effect (see Fig. 10(b)). Furthermore, these data are in broad agreement with the observations by Wijewickreme et al. (2009). Test H4 plots outside the main dataset because of the onerous pinching effect of the rigid platen on the pipe during pressure bag inflation. Apart from this test, the crown of the pipe experiences an initial normal stress that is around 20% higher than the nominal overburden pressure.

Figure 16(b) shows that at the sides of the pipe, there is a clear difference between the present normal stress measurements and those reported by Wijewickreme et al. (2009). They observed average values of the lateral earth pressure coefficient, K , of about 0.5 for loose sand and 1.0 for dense sand, whereas a value of 0.2 is more in keeping with the results of this study. This is possibly attributable to the smaller testing tank used in this work – a width of 0.95 m compared

with 2.5 m in Wijewickreme et al. (2009), giving tank width to pipe diameter ratios of 2.7 and 5.5 respectively.

The redistribution of normal stresses around the pipe circumference during the Hostun sand tests is illustrated in Fig. 17 using polar plots, where the radius at each location (N, S, etc.) denotes the measured normal stress at that point (σ'_N , σ'_S , etc.) normalised by the nominal overburden pressure, σ'_v , at the relevant depth. These plots relate to the stresses immediately prior to testing (Fig. 17(a)), at the peak of the first cycle of cycle set A (Fig. 17(b)), and at the peak of the first cycle of cycle set G (Fig. 17(c)). It is clear that the use of a heavy pipe results in very high initial values of σ'_s for all tests. It can also be seen that there is a significant redistribution of normal stress as the testing progresses; in particular, the initial stresses concentrated at location S appear to be distributed toward the haunches (locations SW and SE) as the pipe settles into the bed layer during the cyclic axial displacements. There is also a significant increase in the normal stresses acting on the sides of the pipe (locations E and W). In all cases except Test H3, the value of the lateral earth pressure coefficient K (i.e. at locations E and W) increases from an initial value of ~ 0.2 to ~ 1.0 towards the end of testing.

Figure 18 shows that the initial normal stresses at the haunches of the pipe are much lower for Sand K than for Hostun sand, and remain low throughout the axial displacement cycles. This is probably due to the compacted bed layer used in the Sand K tests, which limits pipe settlement. Figure 18(c) reveals that for tests K2-K4, the pipe has completely lost contact with the overlying soil during the preceding cycle packets. This confirms that the observed reductions in axial resistance (see Figs 12, 13 and 14(c)) are indeed caused by arching of the compacted damp backfill over the pipe. By contrast in Test K1, with loose damp backfill, there is a significant redistribution of normal stress and the soil remains in contact with the crown and shoulders of the pipe throughout the axial displacement cycles. Considerable settlement

(~70 mm) was observed right across the top surface of the backfill soil during this test, whereas no such surface settlements were seen Tests K2-K4, where arching occurred.

The Stroud cells around the circumference measured both the normal stress σ' and shear stress τ simultaneously, allowing direct assessment of the pipe–soil coefficient of friction, μ . This avoids the need to use of an estimated ‘interface strength reduction factor’, such as that advocated in the ALA approach for the calculation of δ in equation (1). The Stroud cell readings during all of the large axial displacement cycle sets (see Tables 3 and 4) have been plotted as τ against σ' for Hostun sand (Fig. 19(a)) and Sand K (Fig. 19(b)). It can be seen that the inferred coefficient of friction is banded quite well by $0.55 \leq \mu \leq 0.6$ for both soil types, while the measurements from all Stroud cells are very consistent.

AXIAL RESISTANCE PREDICTIONS

ALA approach

Figure 20 shows the measured axial resistances from all tests plotted against predicted resistances obtained using the ALA approach in equation (1). While the ALA code gives no specific guidance on the choice of K_0 in equation (1), it suggests that the value of δ be estimated as $\delta = f\phi'$, where ϕ' is the friction angle of the backfill material and f is an interface strength reduction factor. For the epoxy-coated central section of the test pipe, the minimum recommended value of $f = 0.6$ has been adopted, and peak friction angles of 38° and 36.8° have been selected for Hostun and Sand K, respectively (see Table 1). A value of 0.5 has been assumed for K_0 .

Two separate comparisons with the ALA predicted resistance are presented in Fig. 20: one for the first axial displacement cycle (Fig. 20(a)) and the other for the test maximum and minimum

(Fig. 20b). The terms ‘test maximum’ and ‘test minimum’ denote the largest and smallest peak resistances over all axial displacement cycles performed in a given test, excluding the auxiliary sets of small cycles that were interspersed between the main sets of large cycles. The labels on the data points indicate the corresponding test number. In Test K4, where several different bag pressures were used, the cycle set identifier (see Table 4) is included in parentheses.

For Tests H1 and H2, Fig. 20(a) demonstrates reasonable agreement between the measured data and the ALA predictions. However Tests H3 and H4 highlight the limitations of the model. While the ALA approach predicts the same resistance for both cases, the two tests yielded quite different axial resistances. As discussed above, this discrepancy is believed to arise from trench and pinching effects (see Fig. 10) in Tests H3 and H4 respectively. When considering the maximum and minimum resistances observed in each test (Fig. 20(b)), the agreement deteriorates further. In particular, the occurrence of arching in Tests K2, K3 and K4(A) results in significantly less axial resistance than that predicted using equation (1). Moreover, any apparent agreement is fortuitous given that the ALA approach does not consider the influence of pipe self-weight, which is significant for these tests, particularly the ones at lower overburden pressures. Also, values of $\tan \delta$ obtained from using $f = 0.6$ in the ALA calculation ($\tan \delta = 0.42$ for Hostun sand and 0.41 for Sand K) are significantly smaller than the actual values of the friction coefficient μ inferred from the Stroud cell readings (around 0.6, as shown in Fig. 19).

Alternative methodology

To address these limitations, an alternative design methodology for estimating the axial resistance of a buried pipeline in cohesionless soil was adopted for the field project, based on the equation

$$R_a = \sigma'_N \cdot \beta \cdot \mu \cdot \pi D + \mu \cdot w' \quad (3)$$

where σ'_N is the measured normal stress at the pipe crown prior to any axial displacement, β is a scalar parameter relating the average normal stress around the pipe circumference to that measured at the pipe crown, μ is the measured pipe–soil coefficient of friction, and w' is the pipe self-weight per unit length. By comparison with the ALA approach in equation (1), it can be seen that equation (3) now includes a dedicated term accounting for the contribution of frictional sliding of the pipe under its own weight. Moreover, the measured normal stress at the pipe crown, σ'_N , replaces the nominal overburden pressure at the pipe springline level, $\gamma'H$, while the empirically calibrated parameter β replaces the $(1 + K_0) / 2$ term used in the ALA model. Making β the subject of equation (3) gives

$$\beta = \frac{R_a / \mu - w'}{\sigma'_N \cdot \pi D} \quad (4)$$

Values of the numerator of this expression are plotted against the denominator in Fig. 21. For the first axial displacement cycle (Fig. 21(a)) there is strong linearity in the data, with an average β value of 0.29 for the eight tests reported in this paper. Accounting for the effect of cyclic axial displacements inevitably leads to a more scattered data set because of the need to encompass both the maximum and minimum peak resistances recorded during the course of each test, but from Fig. 21(b) it is clear that β values of 0.6 and 0.2 serve as reasonable upper and lower bounds for the majority of the data. However, these results also highlight the potential for compacted damp backfill to arch over the pipe (Tests K2, K3, K4(A)), thus a value of $\beta = 0$ is a more appropriate lower bound if arching is considered to be a possibility.

Measured values of the initial pipe crown normal stress σ'_N (for various backfill cover depths) are considered to be more appropriate for use within a design method, in lieu of the nominal overburden pressure employed in the ALA approach. These measured values allow for project-specific trench and rigid inclusion effects (Fig. 10) to be incorporated directly into the prediction of axial resistance. These effects are quantified in Fig. 16(a) for the present testing

programme. For application to other projects, laboratory or field measurements of σ'_N specific to the particular soil type and trench configuration could be obtained using a section of the field pipe fitted with basic (i.e. S-beam) compression load cells inside ports along the pipe crown, and monitoring the normal stresses developed during backfilling of a trial trench to various depths.

While the tests described in this paper cover a representative parameter space, additional tests are clearly necessary to extend the scope of the proposed methodology and provide further refinements. These tests could, for example, cover a range of trench width to pipe diameter ratios and trench batter angles, as well as a range of soil types, moisture contents and compaction procedures for the backfill.

CONCLUSIONS

This paper has described the development of a new experimental apparatus for conducting cyclic axial loading tests on a length of buried pipe at full scale. To support the design of a commercial gas pipeline, tests were conducted on a heavy 350 mm diameter pipe in a narrow trench with either dry Hostun sand or damp silty sand as backfill. The tests investigated the axial soil resistance and the distribution of contact stresses around the pipe under a range of boundary conditions, using a pressure bag system to simulate large cover depths where required. The following conclusions arise from the work:

- (a) The influence of axial displacement cycles on the peak axial resistance was shown to depend significantly on the relative density of the backfill. A progressive increase in resistance was observed in loose sand (dry or damp), whereas a drop in resistance was recorded in compacted damp sand.

- (b) The initial normal stress acting on the crown of the pipe was an average of 20% greater than the nominal overburden pressure, indicating a significant rigid inclusion effect. This was comparable to measured data from tests in dry sand documented elsewhere in the literature. By contrast, the initial normal stresses on the sides of the pipe were generally lower than values expected from traditional lateral earth pressure calculations.
- (c) Axial displacement cycles induced a redistribution of the initial normal stresses around the circumference of the pipe. The stresses at the sides of the pipe, in particular, showed notable increases (provided arching did not occur). These results identified much more complex normal stress distributions than the distribution assumed in the industry-standard ALA design approach (ALA-ASCE, 2001).
- (d) Arching of the backfill soil over the pipe was observed in tests where compacted damp sand was used. This was caused by differential settlement of the pipe relative to the backfill during the first few cycles of axial displacement. Surprisingly, a comparable test using loose damp sand exhibited a higher axial resistance, as no arching occurred.
- (e) In one of the tests where arching occurred, an increase in overburden pressure was shown to collapse the arch. This highlights the possibility of a limiting overburden pressure for arch formation, although the observed behaviour could be specific to the test set-up, and in particular the narrow trench configuration, that was used.
- (f) Some limitations of the ALA design approach were identified through comparisons with the present results. The ALA method neglects the influence of pipe weight, provides limited guidance on the choice of interface friction angle, and uses a simplified assumption regarding the normal stress regime around the pipe. In light of this, a revised methodology was proposed for estimating the likely range of axial soil resistance for buried pipelines in sand.

(g) The results of the testing programme have revealed a number of boundary and pipe–backfill interaction effects that influence the axial resistance of a pipeline buried within a narrow trench. Further experimental investigation of these effects, including tests employing other types of backfill soil and other trench configurations (varying both width and batter), would clearly be desirable for future development of the proposed design approach.

ACKNOWLEDGEMENTS

Funding for this research was provided by KW Ltd. The assistance of Mr Clive Baker in the fabrication of the testing rig is also gratefully acknowledged.

543 **NOTATION**

A_r	Pressure bag area ratio
D	External pipe diameter
f	Interface strength reduction factor
h	Height of soil cover measured from the pipe crown
H	Height of soil cover measured from pipe springline (used in ALA-ASCE (2001))
K	Lateral earth pressure coefficient
K_0	Coefficient of lateral earth pressure at rest
p_{bag}	Bag pressure
R_a	Axial resistance (per m length)
w'	Self-weight of the pipe
β	Scalar parameter
γ'	Effective unit weight of the backfill material
δ	Soil-pipe interface friction angle
Δ	Pipe axial displacement
μ	Coefficient of friction
σ'_v	Nominal overburden pressure acting at level of pipe crown
σ'_x	Contact normal stress measured by Stroud X
τ	Contact shear stress
ϕ'	Friction angle of soil backfill

544

REFERENCES

- Ahmed, M. R., Tran, V. D. H. & Meguid, M. A. (2015) On the role of geogrid reinforcement in reducing earth pressure on buried pipes: experimental and numerical investigations. *Soils and Foundations* **55**(3):588-599.
- American Lifelines Alliance - ASCE (2001) *Guidelines for the Design of Buried Steel Pipes*.
- Anderson, C., Wijewickreme, D., Ventura, C. & Mitchell, A. (2004) Full-scale laboratory testing of buried polyethylene gas distribution pipelines subject to lateral ground displacements. In: *Proceedings of 13th World Conference on Earthquake Engineering*, Paper no. 1543.
- Bilgin, Ö. & Stewart, H. E. (2009) Design guidelines for polyethylene pipe interface shear resistance. *Journal of Geotechnical and Geoenvironmental Engineering, ASCE* **135**(6):809-818.
- Brachman, R. W. I., Moore, I. D. & Rowe, R. K. (2000) The design of a laboratory testing facility for evaluating the structural response of small-diameter buried pipes. *Canadian Geotechnical Journal* **37**(2):281-295.
- Bransby, P. L. (1973) *Cambridge contact stress transducers*, Report No. CUED/C-SOILS/LN2, University of Cambridge.
- Colliat, J. L., Desrues, J. & Flavigny, F. (1986) Avantages et inconvénients de l'utilisation d'un système d'antifretage dans l'essai triaxial de compression. *Revue Française de Geotechnique* **34**:41-55.
- Cullin, M. J., Petersen, T. H. & Paris, A. (2015) Corrosion fatigue failure of a gray cast iron water main. *ASCE J. Pipeline Syst. Eng. Pract.* 6(2):05014003.
- Flavigny, E., Desrues, J. & Palayer, B. (1990) Note technique: Le sable d'Hostun. *Revue Française de Geotechnique* **53**:67-70.
- Heron, C. M. (2014) *Note on interface friction*. Report to KW Ltd.
- Huber, M. & Wijewickreme, D. (2014) Response of buried district heating pipelines under relative axial movements In: *Proceedings of Proceedings of the 10th International Pipeline Conference*, pp. 1-5.
- Karimian, S. A. (2006) Response of buried steel pipelines subjected to longitudinal and transverse ground movement. Ph.D. Thesis. The University of British Columbia.

575 Martin, C. M. (1994) Physical and numerical modelling of offshore foundations under
576 combined loads. D.Phil. Thesis. University of Oxford.

577 Scarpelli, G., Sakellariadi, E. & Furlani, G. (2003) Evaluation of soil-pipeline longitudinal
578 forces. *Rivista Italiana de Geotecnica* **4(3)**:24-41.

579 Stroud, M. A. (1971) The behaviour of sand at low stress levels in the simple shear apparatus.
580 Ph.D. Thesis. University of Cambridge.

581 Talesnick, M. L., Xia, H.-W. & Moore, I. D. (2011) Earth pressure measurements of buried
582 HDPE pipe. *Geotechnique* **61(9)**:721-732.

583 Weidlich, I. & Achmus, M. (2006) Reduction of friction forces between soil and buried district
584 heating pipes due to cyclic axial displacements. In: *Proceedings of 10th International*
585 *Symposium on District Heating and Cooling* **16**:18-27.

586 Wijewickreme, D., Karimian, H. & Honegger, D. (2009) Response of buried steel pipelines
587 subjected to relative axial soil movement. *Canadian Geotechnical Journal* **46(7)**:735-752.

588 Wijewickreme, D. & Weerasekara, L. (2015) Analytical modelling of field axial pullout tests
589 performed on buried extensible pipes. *International Journal of Geomechanics* **15(2)**:DOI:
590 10.1061/(ASCE)GM.1943-5622.0000388.

591

Table 1 Sand properties

Property	Hostun HN31	Sand K
Median particle size, D_{50} (mm)	0.35	0.19
Coefficient of uniformity, C_U	1.7	> 2.5
Minimum void ratio, e_{\min}	0.58	0.61
Maximum void ratio, e_{\max}	0.99	0.76
Specific gravity, G_s	2.65	2.67
Peak friction angle, ϕ'_{peak} ($^{\circ}$)	37.9	36.8
Critical state friction angle, ϕ'_{crit} ($^{\circ}$)	35.4	30.5
Optimum moisture content, w_{opt}	-	10.3

592

593

594

595

596

597

598

599

600

Table 2 Summary of samples and boundary conditions

Reference	Material	Moisture content, w (%)	Cover depth, h (m)	Overall unit weight (kN/m ³)	Cover compaction	Test set-up (Fig. 9)	Bag pressure (kPa)	Nominal σ'_v at pipe crown (equation (2)) (kPa)
H1	Hostun	< 1	0.5	13.4	Rained ^a	(i)	n/a	6.9
H2	Hostun	< 1	1.0	13.4	Rained	(i)	n/a	13.7
H3	Hostun	< 1	1.1	13.4	Rained	(ii)	54	50
H4	Hostun	< 1	0.35	13.4	Rained	(iii)	69	50
K1	Sand K	6.2	1.18	13.0	None	(i)	n/a	15
K2	Sand K	6.2	1.18	15.6	Moderate ^b	(i)	n/a	18
K3	Sand K	5.6	1.18	16.4	Full ^c	(i)	n/a	19
K4	Sand K	13.5	0.35	18.5	Moderate	(iii)	20, 51, 83	20, 40, 60

601 ^aSample prepared by raining with no compaction; ^bModerate compaction: spreader board beneath plate compactor; ^cFull
602 compaction: plate compactor directly in contact with soil

603

604

605

606

607

608

609

610

611 **Table 3** Sequence of axial displacement cycles for Tests H1-H4 and K1-K3

Cycle set	Displacement amplitude (mm)	Test:	No. of cycles	
			H1 & H2	H3 & H4; K1-K3
A	20		5	5
B	2		5	5
C	20		5	3
D	2		5	5
E	20		5	3
F	2		5	5
G	20		5	3

612

613

614

615

616

617

Table 4 Sequence of axial displacement cycles for Test K4

Cycle set	Displacement amplitude (mm)	No. of cycles
Pressure bag increase to give $\sigma'_v = 20$ kPa		
A	20	5
Pressure bag increase to give $\sigma'_v = 40$ kPa		
B	20	5
Pressure bag increase to give $\sigma'_v = 60$ kPa		
C	20	5

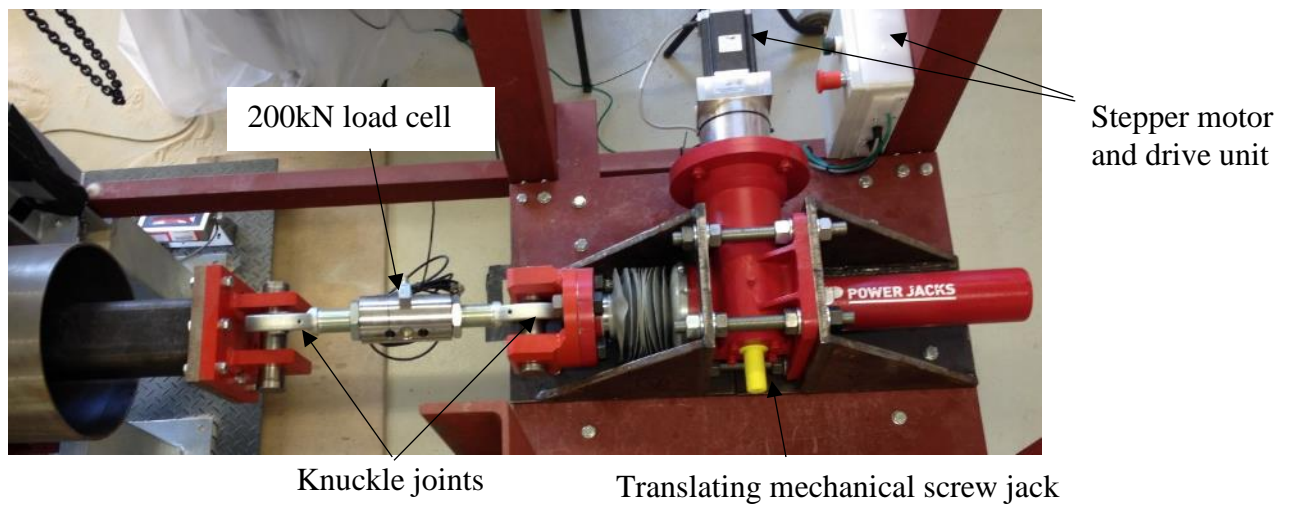
618

619

(a)



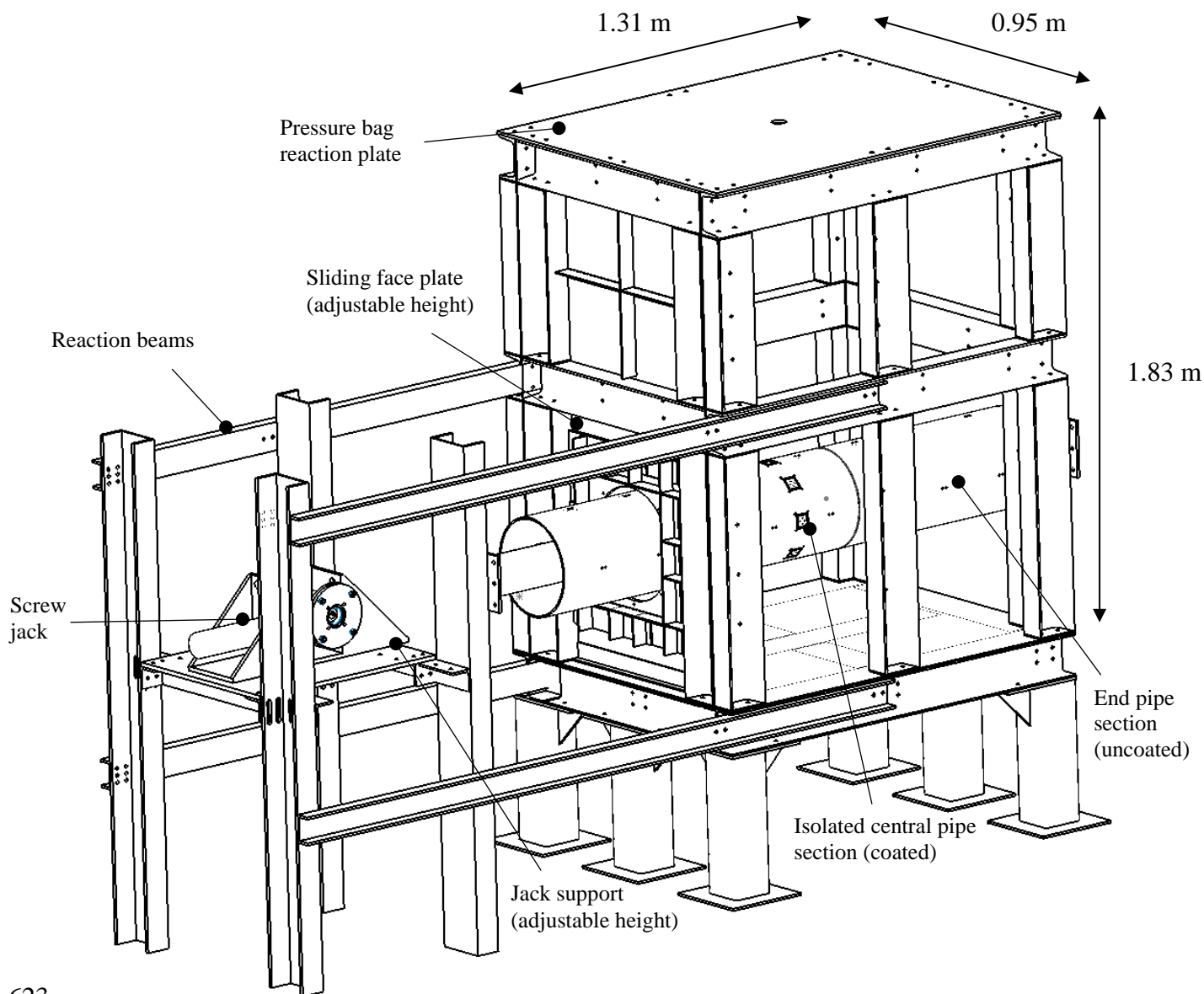
(b)



620

621 **Fig. 1** Buried pipeline testing apparatus: (a) complete rig; (b) close-up of actuation system

622



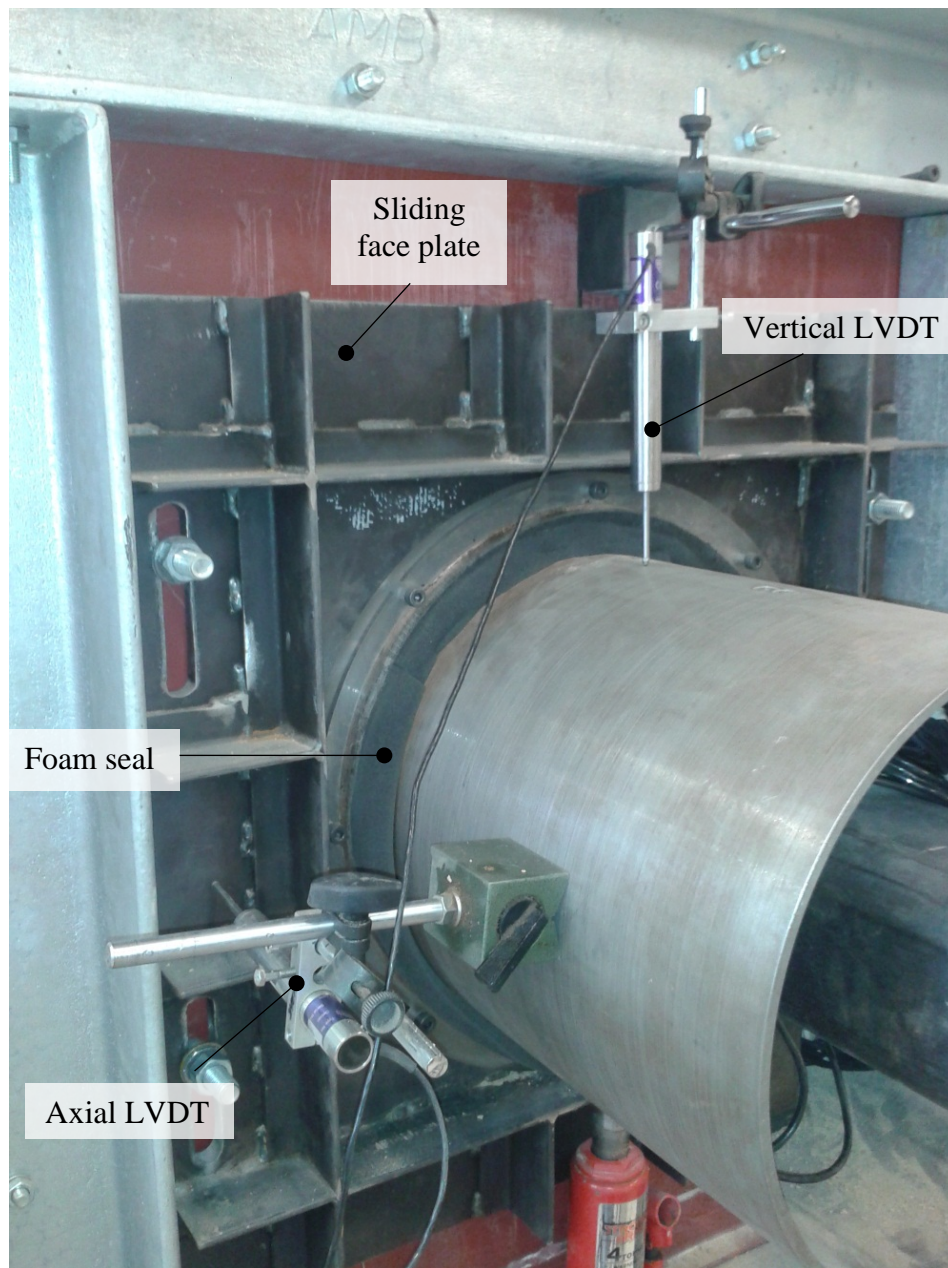
623

624

625 **Fig. 2** Isometric view of testing rig (tank side walls and far end plates not shown);
 626 measurements are internal dimensions of testing tank

627

628



629

630

Fig. 3Sliding face plate with foam seal around pipe

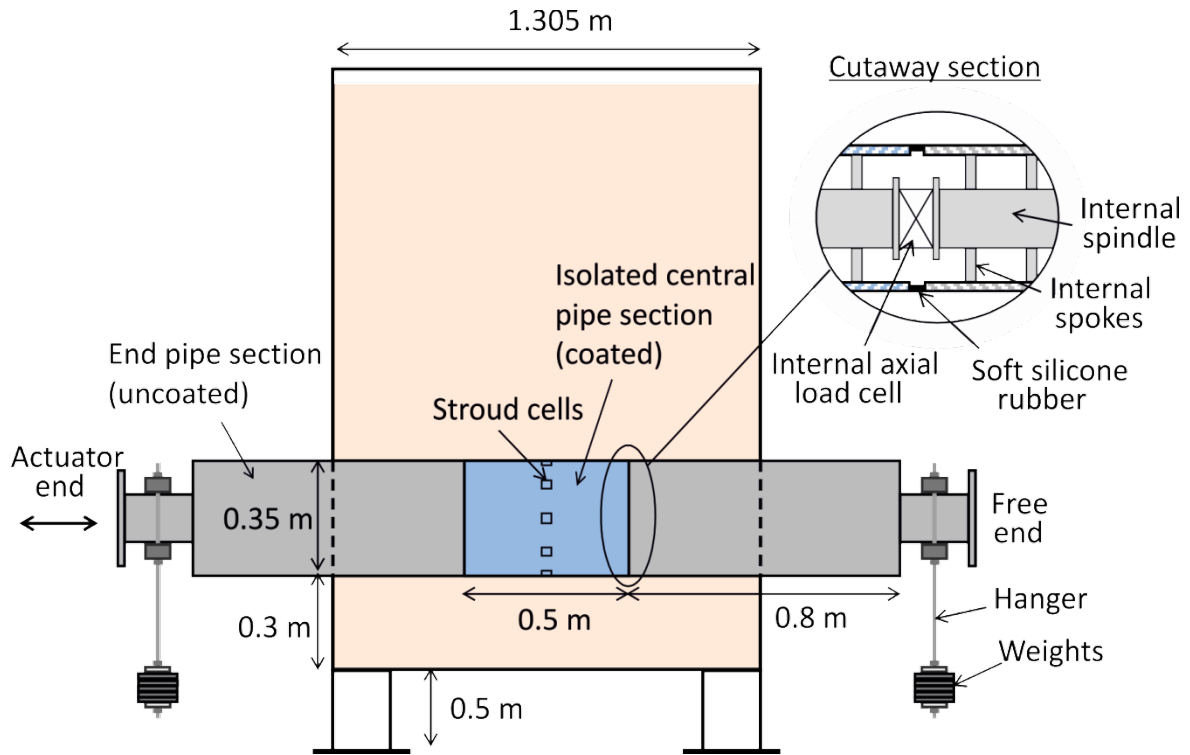
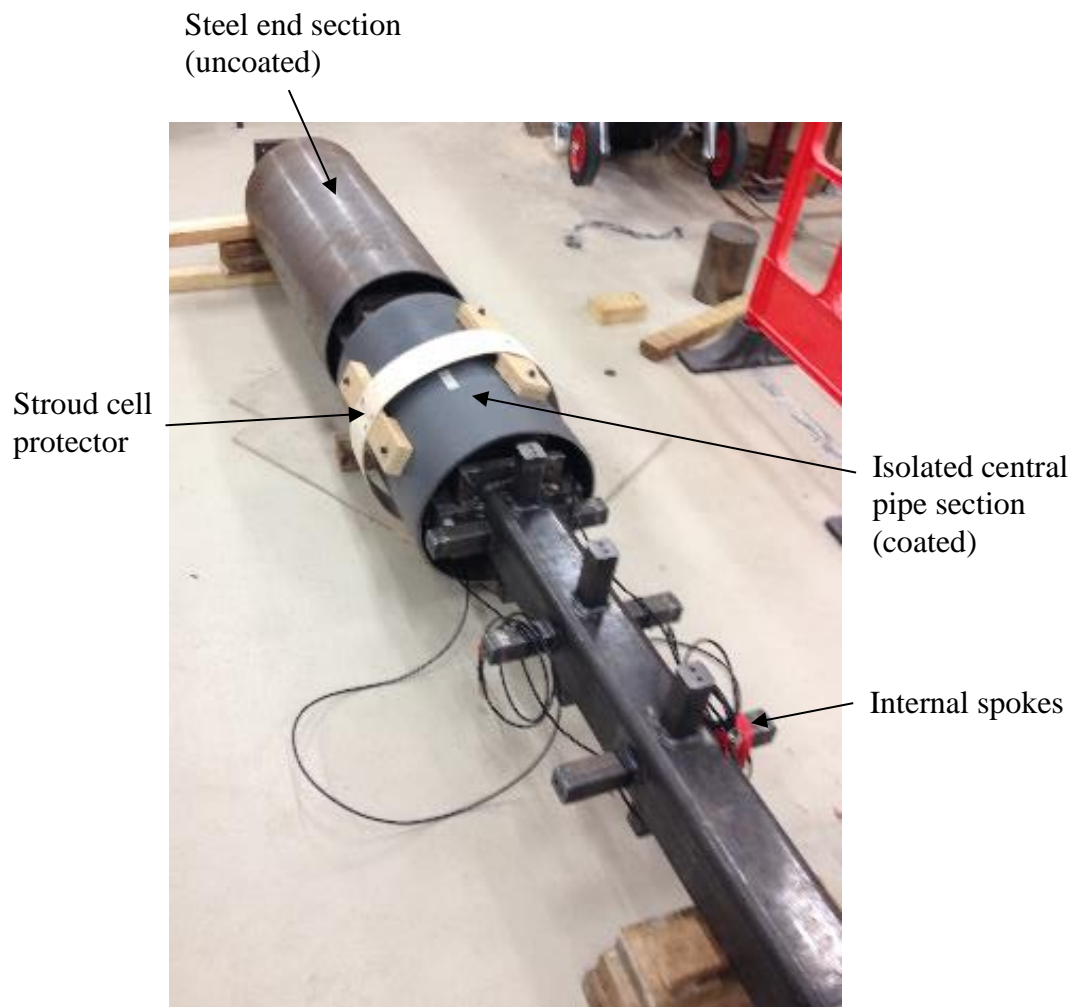


Fig. 4 Front view of test set-up with cutaway section showing internal axial load cell arrangement

637

638



639

640

Fig. 5 Instrumented test pipe during assembly

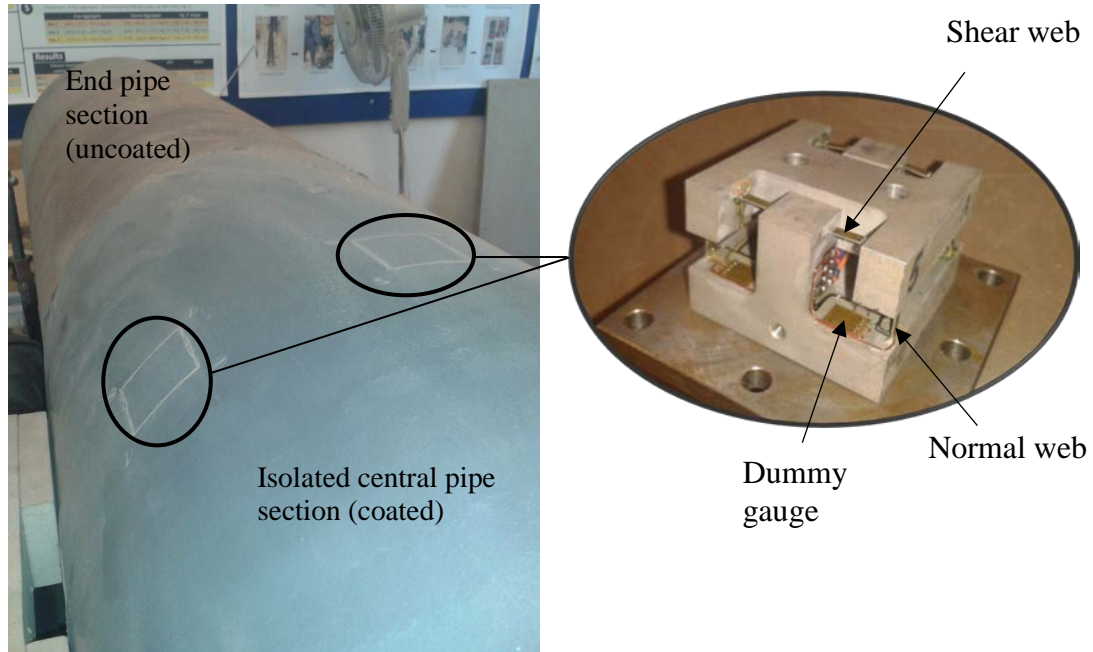


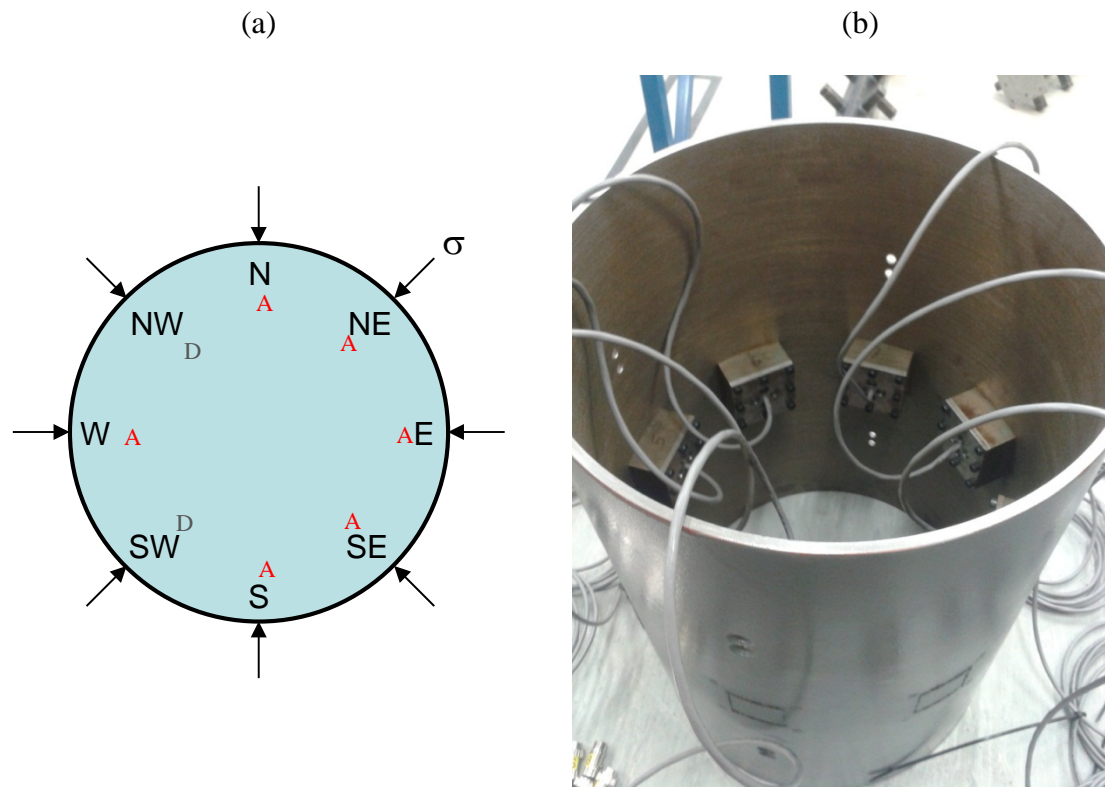
Fig. 6 Stroud load cell, showing slender strain-gauged webs

656

657

658

659



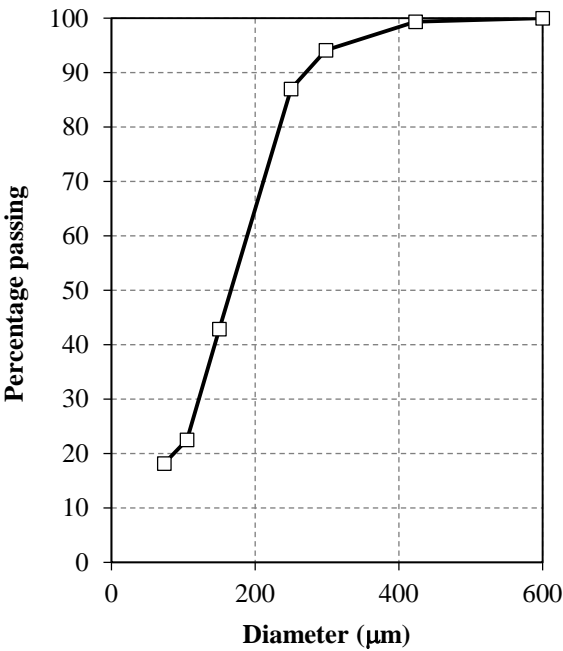
660

661

662

Fig. 7 Locations of Stroud load cells (A = active cell, D = dummy cell)

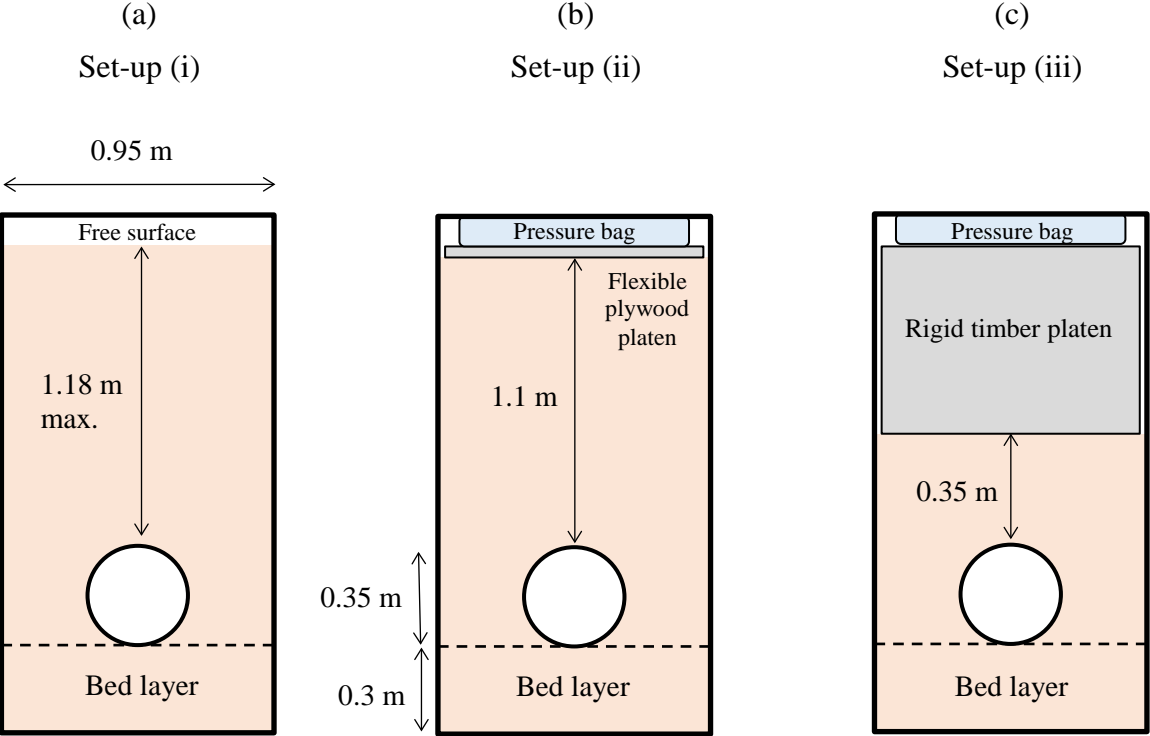
663
664
665



666
667

Fig. 8 Particle size distribution for Sand K

668
669
670

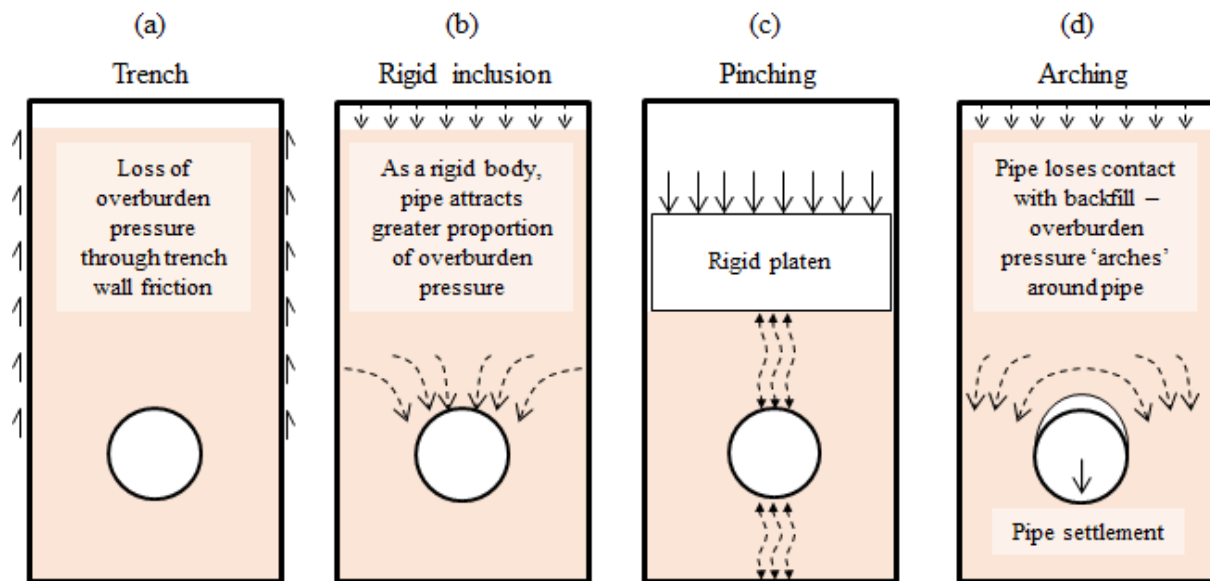


671
672
673

Fig. 9 Test configurations used to vary overburden pressure

674

675

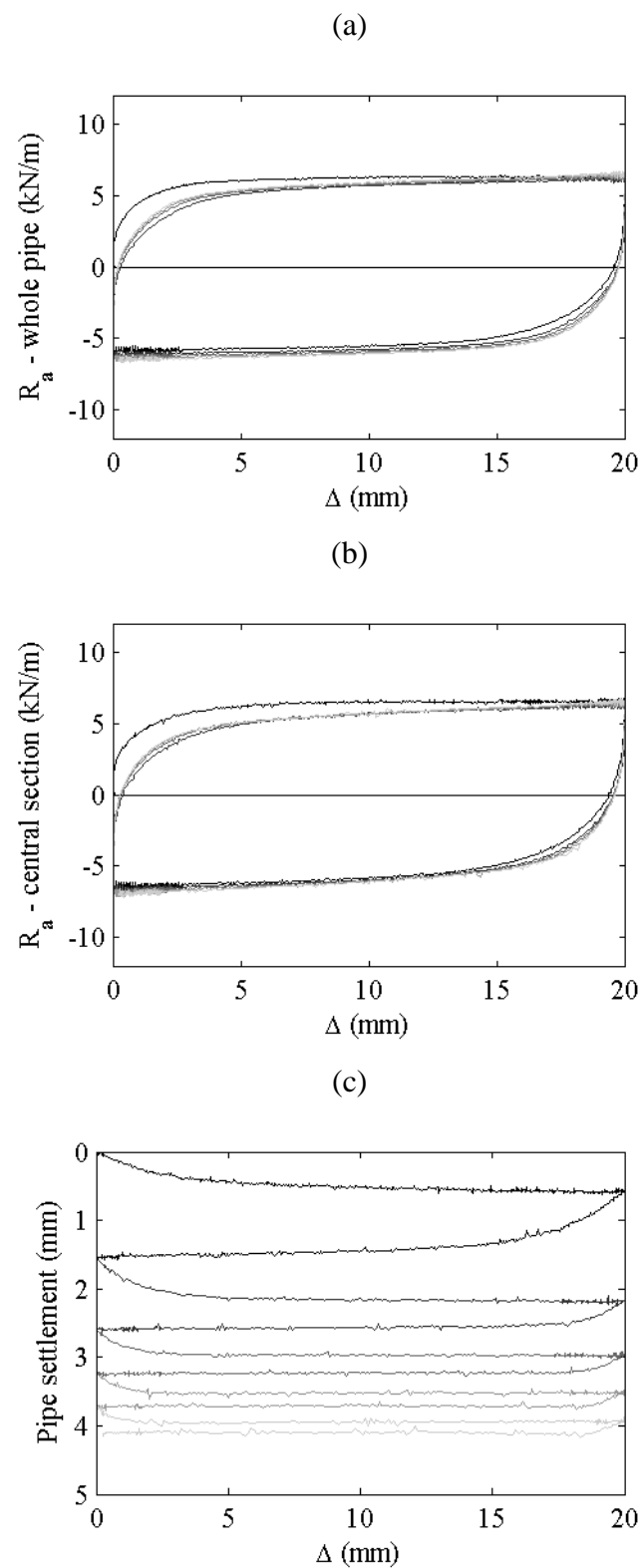


676

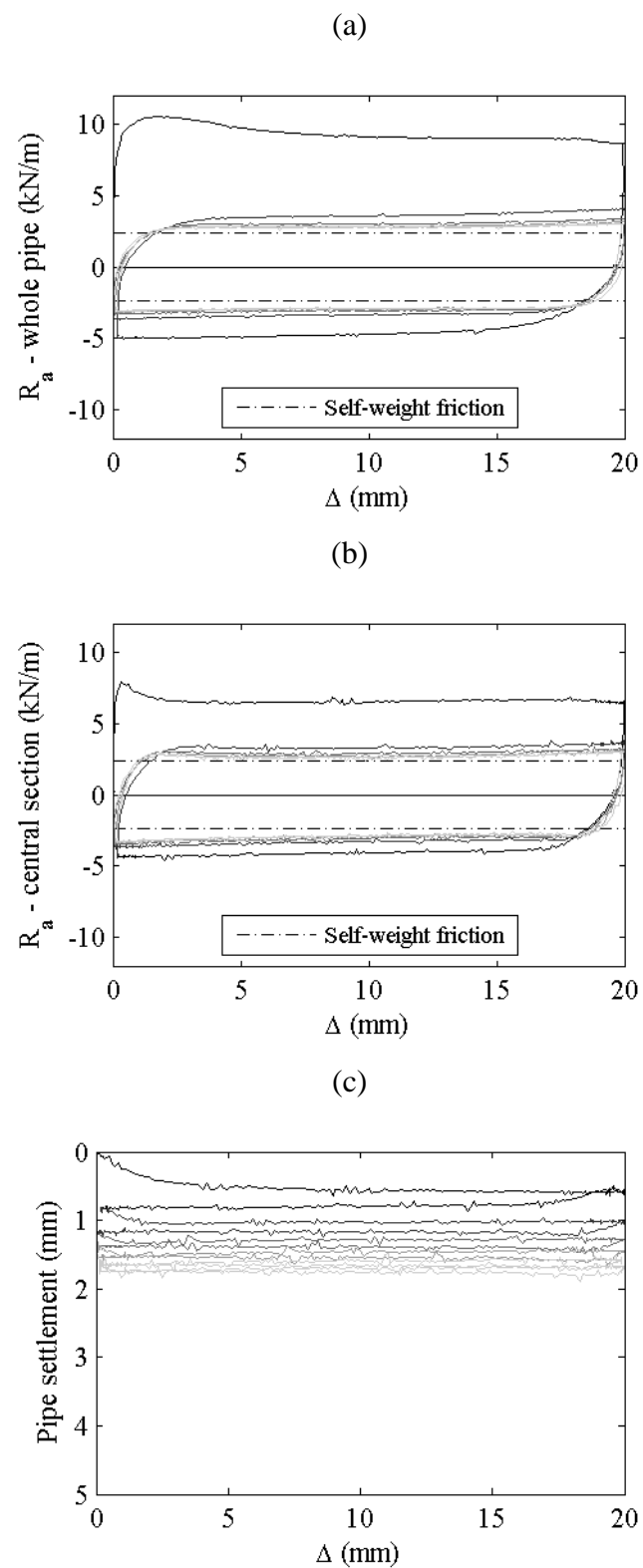
677

678

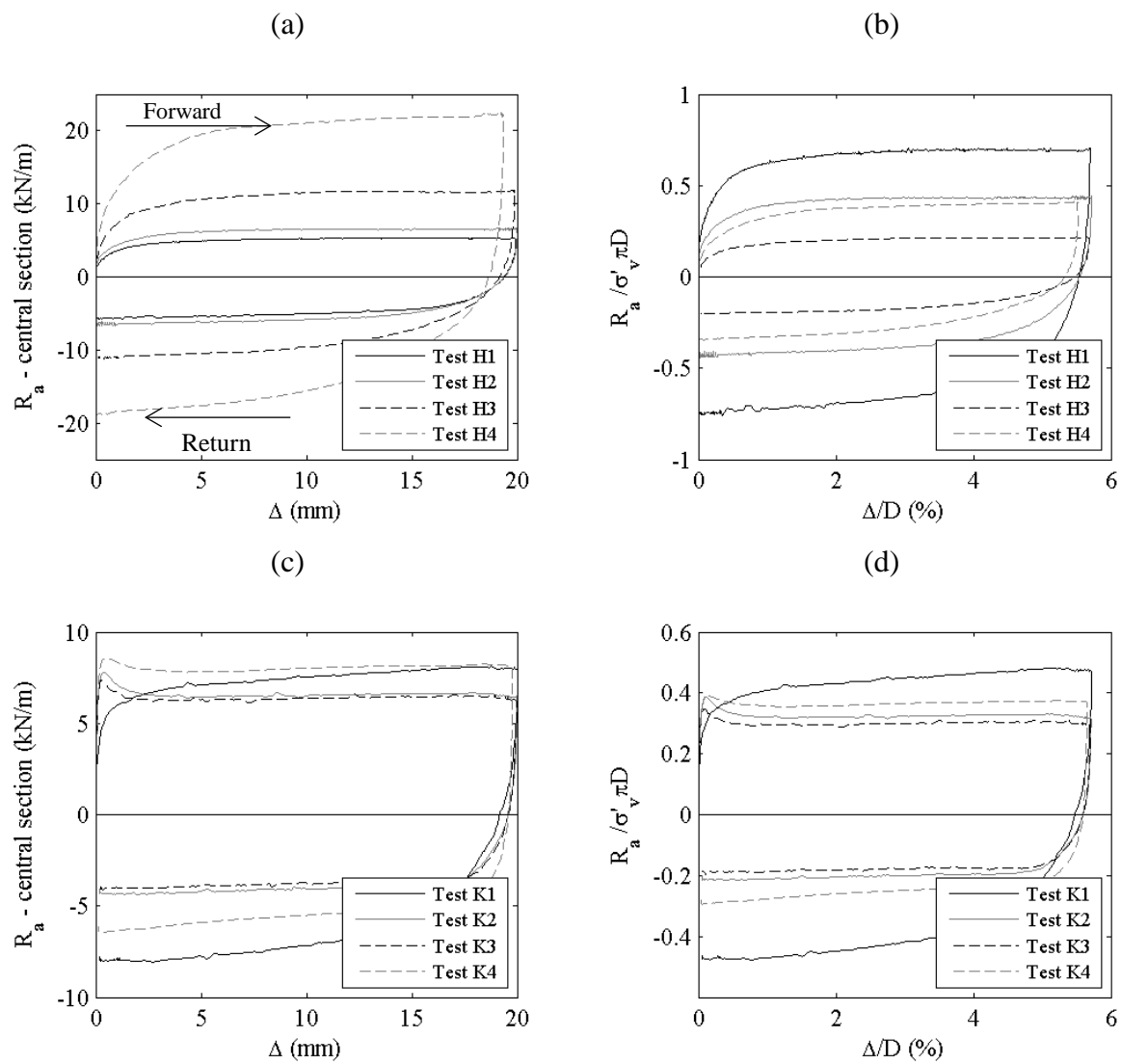
Fig. 10 Schematic of various boundary and pipe–backfill interaction effects



681 **Fig. 11** Results from Test H2, cycle set A: (a) load–displacement (whole pipe), (b) load–
682 displacement (central section), (c) settlement–displacement



685 **Fig. 12** Results from Test K2, cycle set A: (a) load–displacement (whole pipe), (b) load–
686 displacement (central section), (c) settlement–displacement



689 **Fig. 13** Load–displacement response in first cycle: (a) Hostun sand; (b) Hostun sand,
690 normalised; (c) Sand K; (d) Sand K, normalised

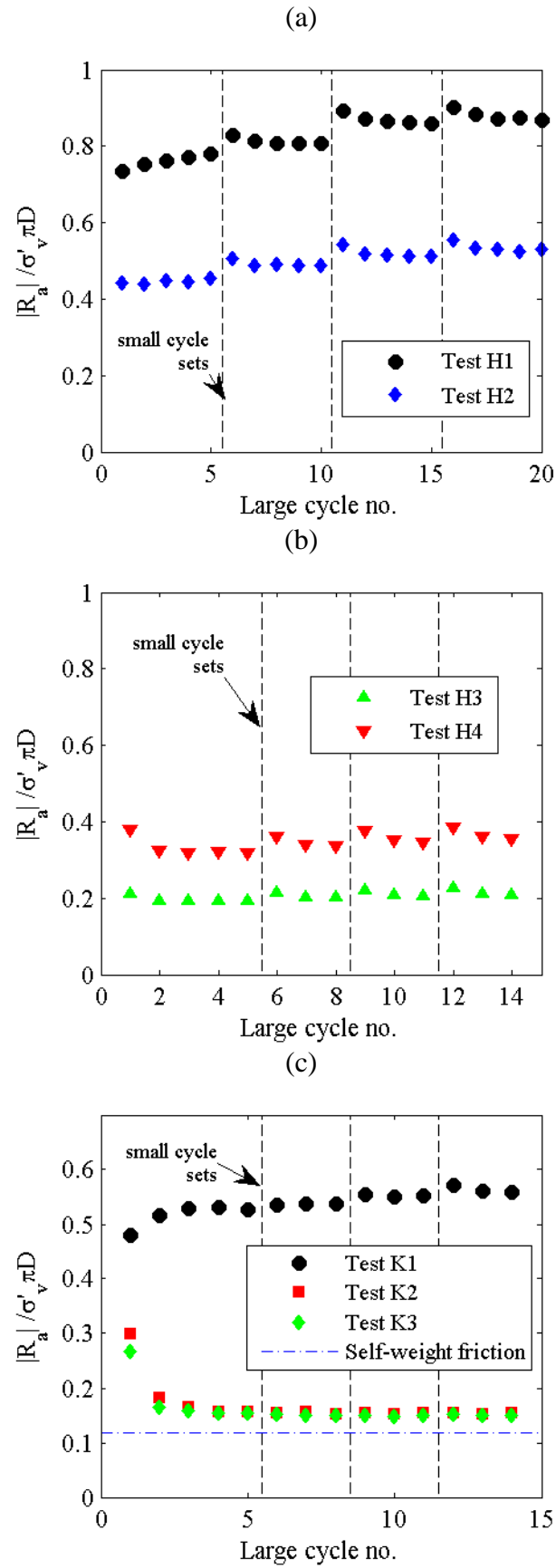
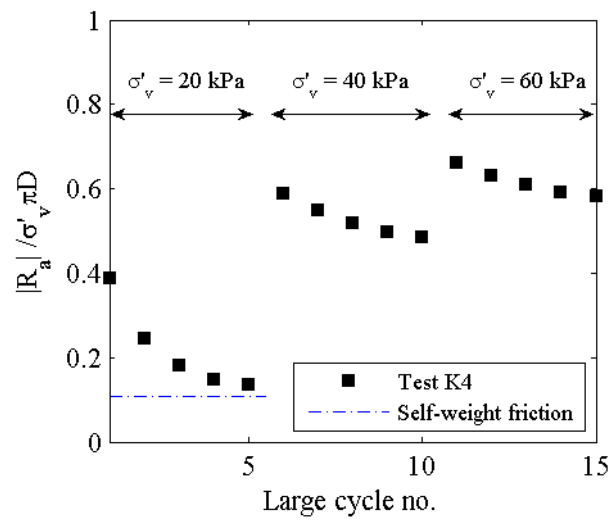


Fig. 14 Influence of axial displacement cycles on normalised peak resistance: (a) Tests H1 and H2; (b) Tests H3 and H4; (c) Tests K1-K3

693
694
695



696
697
698

Fig. 15 Influence of pressure increase phases on normalised peak resistance: Test K4

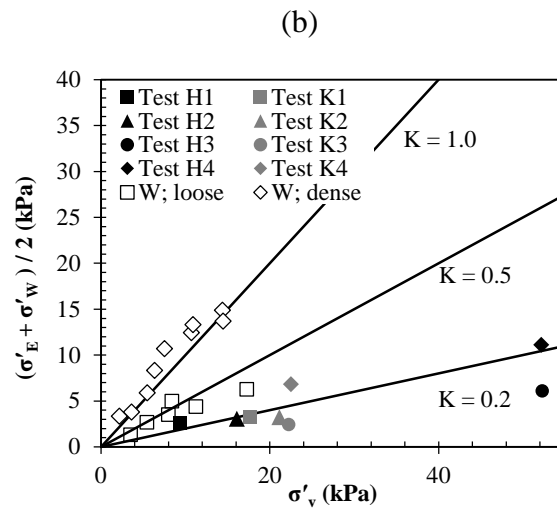
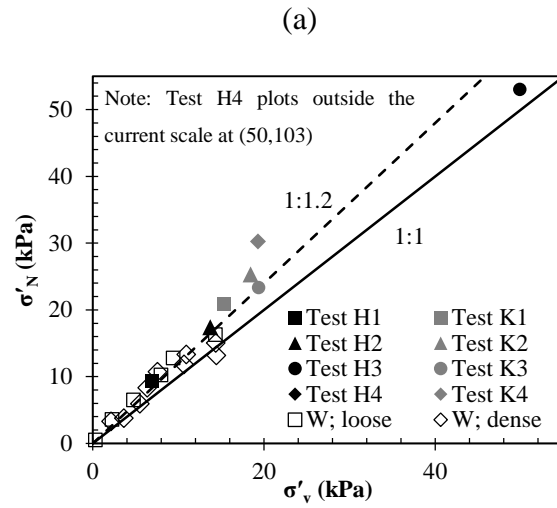


Fig. 16 Initial normal stress measurements versus nominal overburden pressure at Stroud cell locations (a) N and (b) E/W. Data marked W is from Wijewickreme et al. (2009)

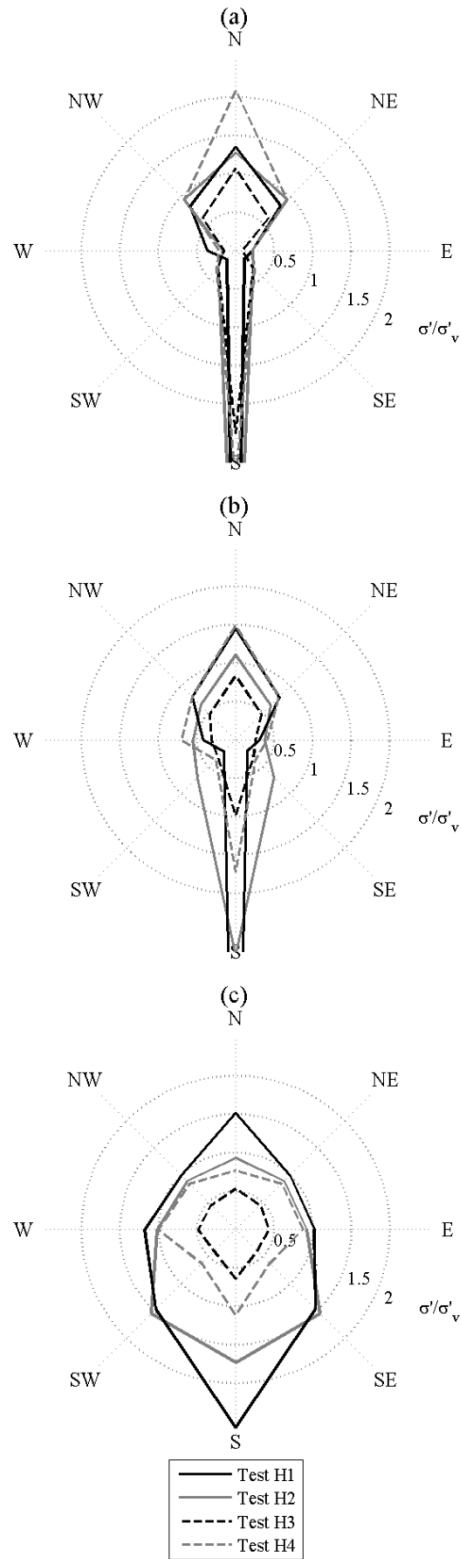


Fig. 17 Polar plots of σ'/σ'_v for Hostun sand tests: (a) initial; (b) peak of first cycle of cycle set A; (c) peak of first cycle of cycle set G

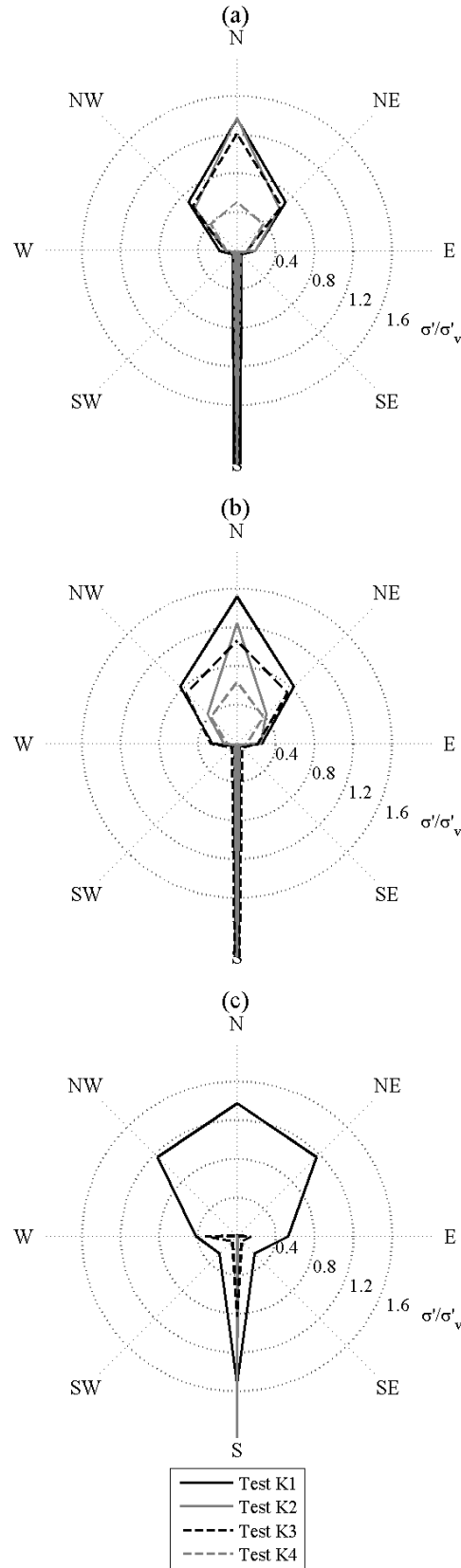


Fig. 18 Polar plots of σ'/σ'_v for Sand K tests: (a) initial; (b) peak of first cycle of cycle set A; (c) peak of first cycle of cycle set G (Test K4 not shown as no small cycles were imposed)

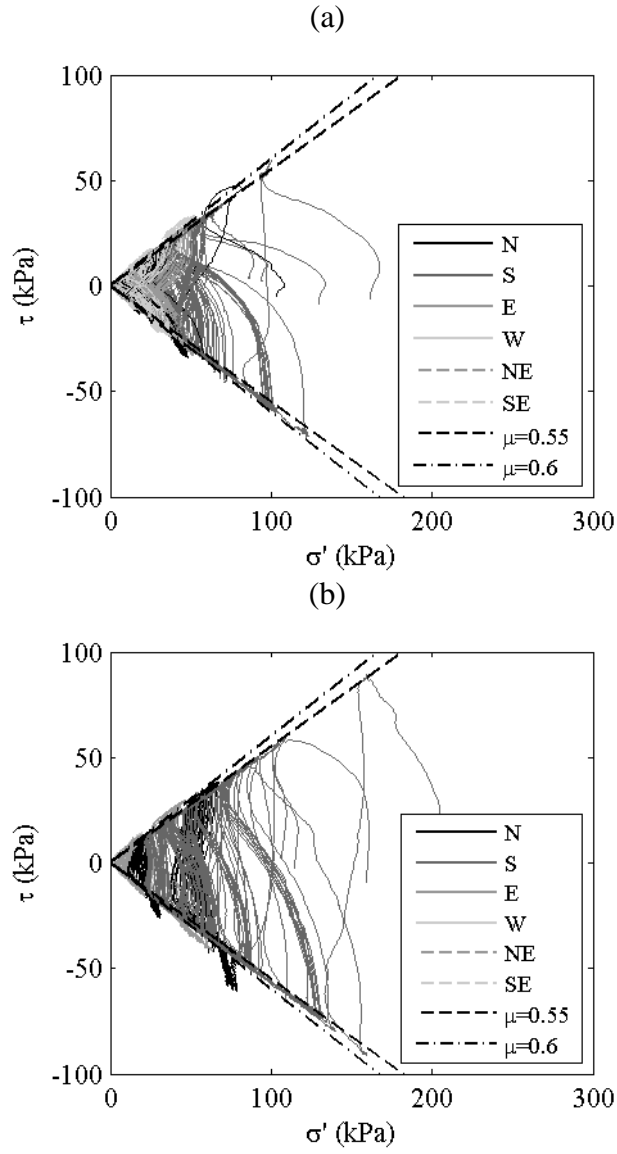


Fig. 19 Contact shear stresses versus normal stresses measured by Stroud cells during large axial displacement cycle sets: (a) Hostun sand; (b) Sand K

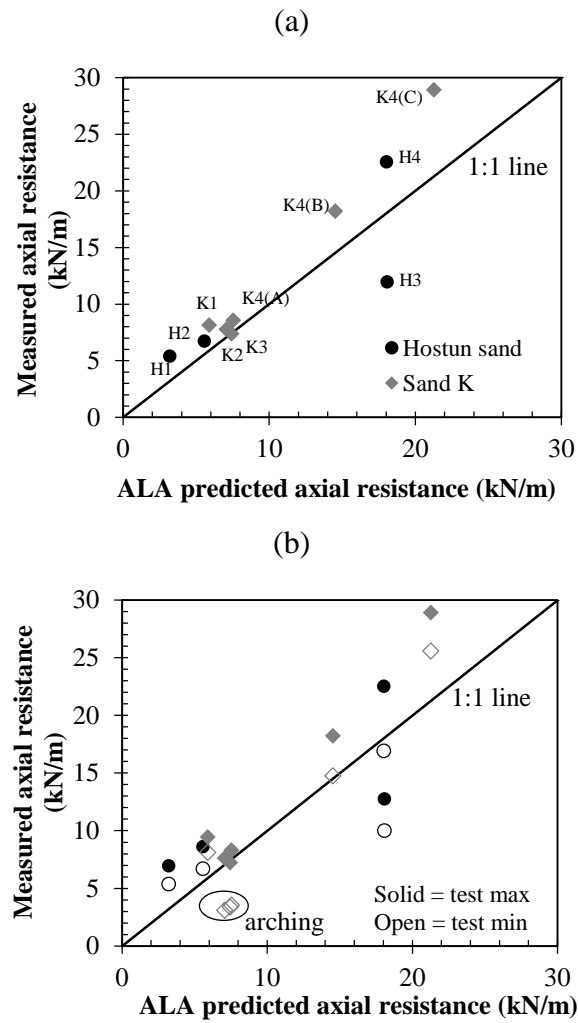


Fig. 20 Comparison between measured axial resistances and predictions from ALA approach (ALA-ASCE, 2001) for all tests: (a) first cycle; (b) test maximum and minimum

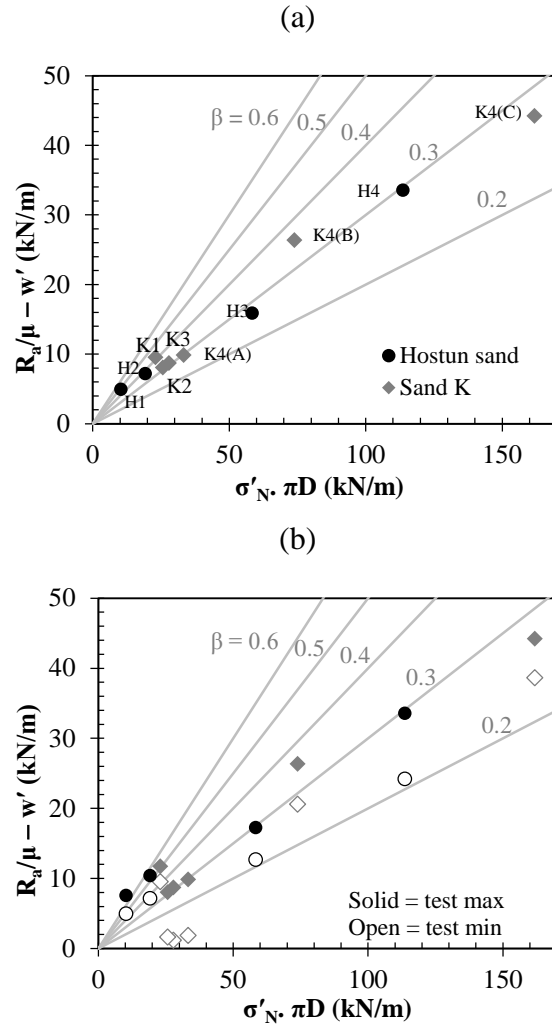


Fig. 21 Calibration of equation (4) for (a) first cycle; (b) test maximum and minimum